Journal of Alloys and Compounds 743 (2018) 419–427

Contents lists available at ScienceDirect

Journal of Alloys and Compounds

journal homepage: http://www.elsevier.com/locate/jalcom

Phase transition and thermoelastic behavior of cadmium sulfide at high pressure and high temperature

Bo Li [a, b], Jingui Xu [a, b], Wei Chen [c], Dawei Fan [a, *], Yunqian Kuang [a, b], Zhilin Ye [a, b], Wenge Zhou [a], Hongsen Xie [a]

[a] Key Laboratory of High Temperature and High Pressure Study of the Earth's Interior, Institute of Geochemistry, Chinese Academy of Sciences, Guiyang 550081, China
[b] University of Chinese Academy of Sciences, Beijing 100049, China
[c] Guizhou Polytechnic of Construction, Guiyang 551400, China

ARTICLE INFO

Article history:
Received 23 November 2017
Received in revised form
11 January 2018
Accepted 2 February 2018
Available online 5 February 2018

Keywords:
Cadmium sulfide (CdS)
High temperature and high pressure
X-ray diffraction
PVT equation of state
Diamond anvil cell (DAC)

ABSTRACT

The phase transition and thermal equation of state of cadmium sulfide (CdS) were studied at high pressure and temperature conditions up to 21.9 GPa and 650 K, by using *in situ* synchrotron angle-dispersive X-ray diffraction and an externally-heated diamond anvil cell (DAC). A pressure-induced phase transition from wurtzite structure (WZ) to rocksalt structure (RS) was observed at about 2.6 GPa, which was agreed with previous studies (2.0–3.5 GPa). In addition, fitting of the experimental data by means of the third-order Brich-Murnaghan equation of state (III-BM EoS) gives the bulk modulus $K_0 = 81.6$ (13) GPa, its pressure derivative $K'_0 = 3.68$ (13), and the volumetric thermal expansion coefficient $\alpha_0 = 2.97\ (25) \times 10^{-5}\,K^{-1}$ for RS phase of CdS. Simultaneously, the thermal expansion coefficient ($\alpha_0 = 1.51 \times 10^{-5}\,K^{-1}$), and its axial thermal expansivities ($8.30 \times 10^{-6}\,K^{-1}$ and $5.96 \times 10^{-6}\,K^{-1}$) along *a*-axis and *c*-axis for WZ phase of CdS at ambient conditions were obtained, respectively. Moreover, it was found that the phase transition pressure from WZ (or ZB) type to RS type of cadmium chalcogenides (CdS, CdSe and CdTe) is quite similar by comparing their phase transition pressures. Furthermore, the elastic properties of metal sulfides (ZnS, CdS, HgS, PbS) with the same crystal structure but different metal cations were also discussed, and found that the bulk moduli for the RS phase of metal sulfides (ZnS, CdS, HgS, PbS) have a negative correlation with the cation radius, but a positive correlation with the electronegativity.

1. Introduction

Cadmium sulfide is the inorganic chemical compound with the formula CdS. It occurs in nature with two different crystal structures as the rare minerals greenockite (wurtzite structure, WZ, Fig. 1A) and hawleyite (zinc-blende structure, ZB, Fig. 1B), but cadmium is more prevalent as an impurity substituent in the similarly structured zinc ores sphalerite and wurtzite [1]. At ambient conditions, greenockite with hexagonal system is the stable phase, while hawleyite with cubic system is thermodynamically unstable [2]. Thus, CdS mainly exist in the form of greenockite at ambient conditions. Greenockite is a rare cadmium sulfide mineral but has the highest cadmium content (up to 77.7%). It is of $P6_3mc$ space group with the lattice parameters are $a = 4.138$ Å and $c = 6.718$ Å [3].

CdS has attained much attention owing to the outstanding photoelectric properties. It is a direct band gap semiconductor because of its 2.4 eV band gap [4]. Because the conductivity of CdS increases when irradiated, it is used to be a photoresistor [4]. And it can be formed the core component of a photovoltaic (solar) and a CdS/Cu_2S solar cell when combined with a *p*-type semiconductor [5,6]. Moreover, CdS crystal can be acted as a soil state laser [7] and both polymorphs of CdS are piezoelectric, but the hexagonal structure polymorph of CdS is also pyroelectric [8]. In addition, CdS is also used as a pigment because of its unique color, good thermal stability, light resistance, chemical resistance and high opacity [9].

To date, the polymorphic structural transformation characteristics of CdS have been extensively studied by experiment and theoretical calculation. Based on previous studies, CdS has a pressure-induced phase transition from WZ phase to RS phase

* Corresponding author.
E-mail address: fandawei@vip.gyig.ac.cn (D. Fan).

https://doi.org/10.1016/j.jallcom.2018.02.021
0925-8388/

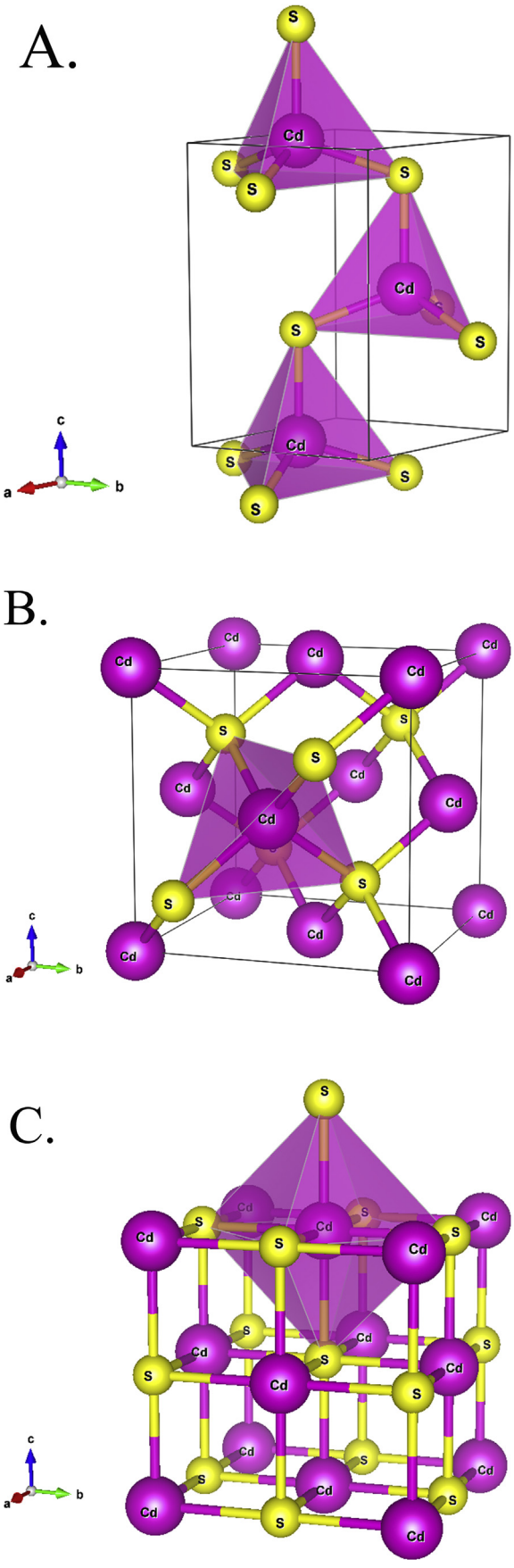

(Fig. 1C) occurred at about 2.0–3.5 GPa [10–26], and accompanied by a change of color from yellow to red [10,17]. By measuring the optical spectra of CdS at high pressure condition, Edwards and Drickamer [10] advocated firstly that the WZ-RS phase transition started at about 2.7 GPa, and essentially completed at about 4 GPa. In a subsequent study, Samara and Drickamer [11] investigated the electrical resistance of CdS and reported that the WZ-RS phase transition occurred at about 2.0 GPa and completed at about 3.0 GPa. Recently, Li et al. [22] also reported the WZ-RS phase transition began at 3.0 GPa and completed at 4.3 GPa based on the results of *in situ* synchrotron radiation X-ray diffraction experiment. However, Zhao et al. [25] obtained the pressure of WZ-RS phase transition for CdS was about 2.7 GPa by Raman scattering experiment, and had not observed the so-called two-phase mixing phenomenon in the range of 3.0–5.3 GPa. To sum up, the exact phase transition pressure of CdS is still controversial, especially for the mixed WZ-RS structure in the WZ-RS phase transition process.

During the past few decades, many previous studies including experiment and theoretical calculation have been carried out on the elastic properties (bulk modulus (K_0) and its pressure derivative (K'_0)) of CdS. But these results were not consistent each other, the values for K_0 of WZ phase of CdS range from 62.8 [19] to 79.48 GPa [18], and the K_0 values for RS phase of CdS span from 86.7 [24] to 105 GPa [22]. Furthermore, experimental measurements on the elasticity of CdS at high pressure and high temperature remain lacking [2,23,27]. By measuring the electrical resistance, Osugi et al. [23] investigated the WZ-RS phase transition of a single crystal of CdS over a *P*, *T* range of about ~2.5 GPa and ~973 K, and reported that the transition pressure was lowered with increasing temperature and the WZ-RS phase boundary had a slope of 1020 K/GPa. Recently, Zhou et al. [2] studied the thermodynamic properties of CdS by employing first principle and a quasi-harmonic Debye model and reported that the heat capacities of WZ phase and RS phase of CdS decrease with pressure and increase with temperature. Similarly, Xiao et al. [27] investigated the high temperature and high pressure phase diagram and phase transformation pathways of CdS by using density functional theory combined with a quasi-harmonic approximation method. Overall, the studies of the thermodynamic properties of CdS are mainly limited to theoretical calculations over the past 20 years.

In summary, the pressure-induced phase transition and the elastic properties of CdS at high pressure and room temperature conditions have been studied extensively, but these results are not consistent each other. Moreover, to the best knowledge of the authors, there is still no experimental investigation about the *PVT* equation of state of CdS, which has great significance to understand the phase transition, thermophysical properties and structural changes of sulfide minerals. Therefore, in this study, we investigated the *P-V-T* relations of CdS at high pressure and high temperature up to 21.9 GPa and 650 K, using an externally-heated DAC combined with *in situ* synchrotron radiation angle-dispersive X-ray diffraction (ADXD). The phase transition process and *PVT* equation of state of CdS at high pressure and high temperature conditions were obtained. In addition, the phase transition pressures of cadmium chalcogenides (CdS, CdSe and CdTe) transforming from WZ (or ZB) type to RS type were compared. Furthermore, the elastic properties of different metal sulfides XS (X = Zn, Cd, Hg, Pb), which have the same structure, were also compared. Moreover, the effects

Fig. 1. Crystal structures of cadmium sulfide. Purple and yellow spheres stand for Cd and S atoms, respectively. A, B and C is represented wurtzite structure, zinc-blende structure and rocksalt structure, respectively. (For interpretation of the references to color in this figure legend, the reader is referred to the Web version of this article.)

of electronegativity and cationic radius on bulk modulus of metal sulfide were also discussed.

2. Sample and experimental methods

2.1. Sample

The cadmium sulfide sample selected for this investigation is high purity (99.99%) powder sample that purchased from Alfa Aesar Corporation. The powder samples were examined using the conventional powder X-ray diffraction method, after being heated at 50 °C in a constant temperature furnace for 2 h to eliminate the absorbed water. The ambient X-ray diffraction data were collected using a D/Max-2200 X-ray diffractometer with graphite crystal monochromator and Cu Kα radiation. The ambient X-ray spectrum of CdS sample was indexed according to the standard spectra, confirming that the structure of the CdS is hexagonal, and belongs to the $P6_3mc$ space group.

2.2. Room-temperature and high-pressure X-ray diffraction experiment

The *in situ* room-temperature and high-pressure angle-dispersion X-ray diffraction experiments were carried out at BL15U1 beamline of Shanghai Synchrotron Radiation Facility (SSRF). The incident synchrotron X-ray beam was monochromatized to a wavelength of 0.6199 Å and focused down to $2 \times 3\ \mu m^2$. A symmetric piston cylinder DAC equipped with 500-μm diamond culets was used. Rhenium tablet was used as gasket, and a hole with a diameter of 300 μm drilled in the gasket, worked as the sample chamber. The Neon gas was filled in the chamber as a pressure-transmitting medium [28]. Ruby chip was loaded as calibrant of pressure together with the CdS sample in the sample hole. The fluorescence spectrum of ruby was collected before and after each collection of data, and the positions of R1 and R2 were determined by fitting with Lorentzian function, and then the experimental pressure was calculated [29]. Diffraction images of the samples were collected using a MAR-165 charge-coupled device (CCD) detector. The sample-to-detector distance and the geometrical parameters of the detector were calibrated with the cerium dioxide (CeO_2) powder as the X-ray diffraction standard. Typical exposure time for collecting diffraction images of the sample was 500 s. In order to obtain conventional one-dimensional diffractive patterns, all collected images were integrated as a function of 2θ using the *Fit2D* program [30]. And the diffraction peak positions were fitted by using the *Origin 8.5* software. And then the unit cell parameters of CdS (Tables 1 and 2) were calculated and refined by using the *UnitCell* software [29]. Finally, the EoS of CdS was fitted by using the *EoSFit 5.2* software [31].

Table 1
Unit cell parameters of cadmium sulfide in wurtzite structure at atmospheric pressure and high temperature.

P(GPa)	*T*(K)	*a*(Å)	*c*(Å)	*V*(Å^3)
0.0	300	4.1332(7)	6.713(2)	99.32(3)
0.0	350	4.1349(7)	6.712(2)	99.39(3)
0.0	400	4.1363(6)	6.713(2)	99.46(3)
0.0	450	4.1364(7)	6.714(2)	99.50(3)
0.0	500	4.1377(7)	6.716(2)	99.57(3)
0.0	550	4.1391(7)	6.716(2)	99.65(3)
0.0	600	4.1396(5)	6.720(2)	99.73(3)
0.0	650	4.1421(5)	6.720(2)	99.84(3)

The numbers in parentheses are 1σ uncertainties on the last digits.

Table 2
Unit cell parameters of cadmium sulfide in rocksalt structure at various *P-T* conditions.

P(GPa)	*T*(K)	*a*(Å)	V(Å^3)
2.6	300	5.3973(6)	157.23(5)
3.2	300	5.3837(5)	156.04(5)
4.1	300	5.3634(5)	154.29(5)
5.0	300	5.3542(5)	153.49(5)
6.2	300	5.3303(6)	151.44(5)
7.1	300	5.3142(6)	150.08(5)
8.2	300	5.2973(6)	148.65(5)
9.0	300	5.2840(6)	147.53(5)
10.1	300	5.2699(6)	146.35(5)
10.9	300	5.2573(6)	145.31(5)
12.0	300	5.2405(6)	143.92(5)
13.0	300	5.2271(6)	142.82(5)
14.2	300	5.2093(6)	141.36(5)
16.2	300	5.1844(6)	139.35(5)
17.9	300	5.1626(6)	137.59(5)
19.5	300	5.1440(6)	136.11(5)
20.9	300	5.1295(6)	134.97(5)
21.9	300	5.1175(6)	134.02(5)
4.4	350	5.3606(7)	154.04(6)
4.7	400	5.3578(6)	153.80(6)
5.0	450	5.3548(6)	153.54(6)
5.1	500	5.3559(6)	153.63(6)
5.4	550	5.3544(6)	153.50(6)

The numbers in parentheses are 1σ uncertainties on the last digits.

2.3. High-temperature and high-pressure, and high-temperature and room-pressure X-ray diffraction experiments

High-temperature and high-pressure, and high-temperature and room-pressure experiments were carried out by using an externally-heating DAC [32]. A pair of 500-μm-culet-size diamond anvil was used. Gasket made from stainless-steel foil (type T301), which was pre-pressed to a thickness of 60–80 μm and then drilled to a diameter of 200–300 μm served as the sample chamber. Heating was carried out by using a NiCr resistor wire with a diameter of 0.3 mm as an external heating device. The temperature was measured by a $Pt_{90}Rh_{10}$-Pt_{100} thermocouple connected to the pavilion of the diamond, and its precision was ±2 °C. For high-temperature and high-pressure experiment, Au powder was employed as the pressure calibrant [33], which completely mixed with the CdS powder in a 5% ratio by mechanically grinding for approximately 4 h. Then, the blended powder was slightly pressed with two opposing diamond anvils to form an approximately 25-μm-thick disk, and a piece of sample about 100 μm in diameter was loaded into the sample chamber. The 16:3:1 mixture of methanol-ethanol-water was used as the pressure-transmitting medium [34]. We first compressed the sample up to about 4.0 GPa at room temperature, and then increased the temperature from 300 K to 550 K in 50 K steps. In order to minimize the effect of non-hydrostatic stress that could develop upon cold compression, the spectrums were selected after the experiment temperature maintained for about 600 s. For high-temperature and room-pressure experiment, CdS powder was slightly pressed to form an approximately 50-μm-thick disk, and a piece of sample about 200 μm in diameter was loaded into the sample chamber. No pressure-transmitting medium was used. The experimental process of this experiment is as follows. The temperature is firstly increased from room temperature to the maximum temperature of 650 K, and then heating was kept for ~600 s in order to relax the sample before collection of the powder diffraction spectrum. Next, the temperature was lowered down to 300 K in 50 K steps. For each *P-T* condition, an X-ray diffraction pattern was collected, and the typical exposure times for collecting diffraction patterns of the sample and

the pressure marker were 200 s. Details of the experimental setup and cell assembly were described in Fan et al. [32].

In situ high-temperature and high-pressure, and high-temperature and room-pressure powder X-ray diffraction experiments were conducted at the 4W2 beamline of Beijing Synchrotron Radiation Facility (BSRF). An image plate detector (MAR-345) was used to collect diffraction patterns. The incident X-ray beam was monochromatic with a wavelength of 0.6199 Å calibrated by scanning through the Mo metal *K*-absorption edge. The X-ray beam was focused to a beam size of $20 \times 30\ \mu m^2$ full width at half maximum by a pair of Kirkpatrick-Baez mirrors. The tilting and rotation of the detector relative to the incident X-ray beam were calibrated using CeO_2 powder as the X-ray diffraction standard. And the sample-detector distance was calculated from the CeO_2 powder at ambient conditions. Diffraction patterns were integrated and processed as same as room-temperature and high-pressure X-ray diffraction experiment done.

3. Experimental results

The X-ray diffraction pattern at different *P-T* conditions in this study is shown in Fig. 2, and the characteristic diffraction peaks of CdS in WZ type are (100), (002), (101), (102), (110), (103) and (112) (Fig. 2A). As the pressure increases to about 2.6 GPa, the X-ray diffraction patterns of CdS changes obviously, and the original diffraction peaks disappeared completely with the advent of new diffraction peaks, which indicates that the CdS has a phase transition and changes completely from the WZ phase to the RS phase. The characteristic diffraction peaks of the RS phase are (111), (200), (220), (311), and (222) (Fig. 2B and C). Moreover, CdS still maintains the RS phase structure at the maximum experimental pressure in this study (~21.9 GPa).

3.1. Pressure-volume date of RS phase of CdS at room temperature

The unit cell parameters of the WZ phase and the RS phase for CdS at different *P-T* conditions are shown in Tables 1 and 2. Since the *P-V* data of the WZ phase are relatively scarce, which will produce a large error by fitting the EoS, and the *P-V EoS* for the RS phase of CdS is fitted solely here.

According to the III-BM EoS [35]:

$$P = \frac{3}{2}K_0\left[(V_0/V)^{\frac{7}{3}} - (V_0/V)^{\frac{5}{3}}\right] \times \left[1 + \frac{3}{4}(K_0' - 4)\left[(V_0/V)^{\frac{2}{3}} - 1\right]\right] \quad (1)$$

where V_0, V, K_0 and K'_0 represent the zero-pressure unit cell volume, high-pressure unit volume, the zero-pressure isothermal bulk modulus and its pressure derivative, respectively. Analyses of Eq. (1) with all parameters free yield $V_0 = 162.01\ (11)$ Å^3, $K_0 = 81.6\ (13)$ GPa, $K'_0 = 3.68\ (13)$ for RS phase of CdS. With fixed K'_0 at 4, the fitting results yield $V_0 = 162.25\ (7)$ Å^3, $K_0 = 78.4\ (4)$ GPa, respectively. Fig. 3 shows the volume compression (V/V_0) of RS phase of CdS as a function of pressure (P) and the derived III-BM EoS. To evaluate the quality of the III-BM EoS fitting acquired from the plot of unit cell volume against pressure, the relationship between the Eulerian strain ($f_E = [(V_0/V)^{2/3} - 1]/2$) and the normalized pressure ($F_E = P/[3f_E(2f_E + 1)^{5/2}]$) was plotted and shown in Fig. 4 [31]. The weighted linear regression through the data points yields the intercept $F_E(0) = 81.6\ (4)$ GPa, which shows a perfect agreement

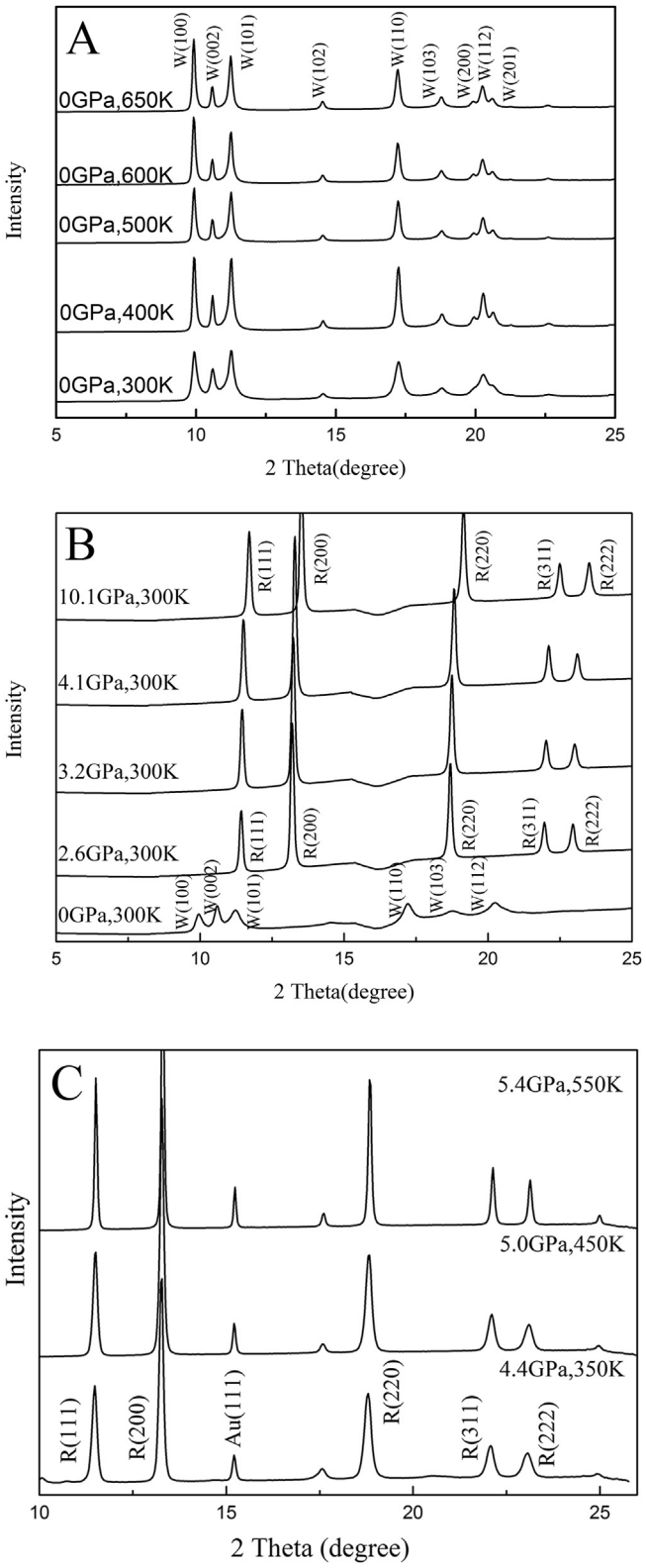

Fig. 2. Representative X-ray diffraction patterns of cadmium sulfide under the *P-T* conditions (A: high-temperature and room-pressure, B: room-temperature and high-pressure, C: high-temperature and high-pressure) indicated. W: wurtzite phase peak; R: rocksalt phase peak.

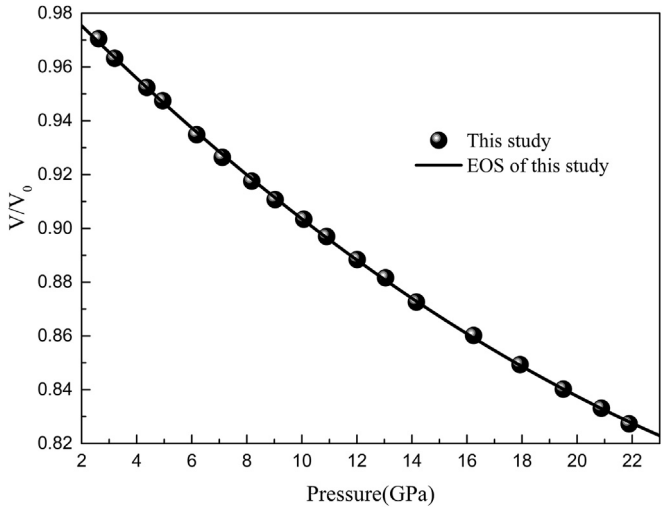

Fig. 3. P–V data of cadmium sulfide in rocksalt structure at room temperature.

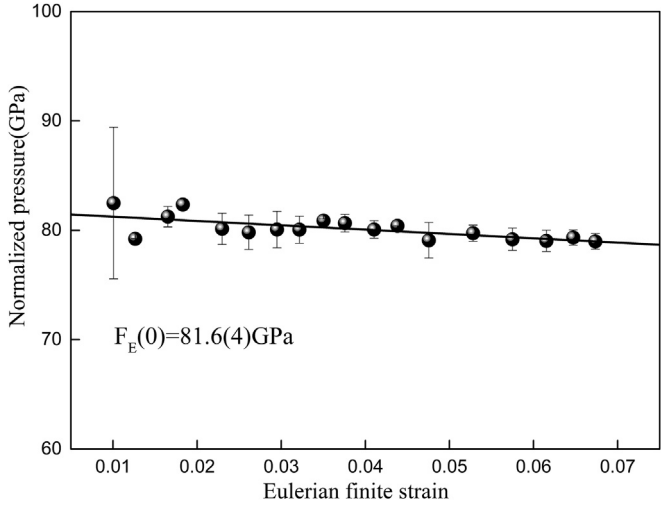

Fig. 4. vol Eulerian strain-normalized pressure (F_E-f_E) plot of cadmium sulfide in rocksalt structure.

with the isothermal bulk modulus obtained by the III-BM EoS (81.6 (13) GPa). Additionally, it is identified from Fig. 4 that the normalized pressure as a function of the Eulerian strain at 300 K has a negative slope, which is consistent with a value of K'_0 slightly smaller than 4 [31]. Therefore, the relationship between the Eulerian strain and normalized pressure indicates that the III-BM EoS is a reasonable description of the *P-V* data in this study.

3.2. Temperature-volume data for WZ phase of CdS

The *T-V* data (Table 1) were used to determine the thermal expansion coefficient of WZ phase for CdS up to 650 K at ambient pressure. The thermal expansion expression proposed by Fei [36] was applied to our room-pressure and high-temperature data in the form as follows:

$$V_{0T}=V_0 exp\left[\alpha_0(T-300)+1/2\alpha_1\left(T^2-300^2\right)-\alpha_2\left(\frac{1}{T}-\frac{1}{300}\right)\right] \quad (2)$$

where V_0 represents the unit cell volume at temperature of300 K, and α_0, α_1, α_2 are the parameters for the thermal expansion α_T as a function of temperature ($\alpha_T=\alpha_0+\alpha_1 T+\alpha_2 T^{-2}$ (with *T*in Kelvin)). By fitting Eq. (2) using the unit cell parameters in this study, we obtained the thermal expansion $\alpha_T=-4.13\times10^{-5}+8.86\times10^{-8}T+2.68\ T^{-2}$ for WZ phase of CdS. So the α_T of WZ phase of CdS at ambient conditions is $1.51\times10^{-5}\,K^{-1}$ (Fig. 5). In addition, we also obtained the axial thermal expansivities of CdS in WZ phase along *a*-axis and *c*-axis is $\alpha_{aT}=-3.71\times10^{-5}+6.43\times10^{-8}T+2.35\ T^{-2}$ and $\alpha_{cT}=-1.05\times10^{-5}+2.19\times10^{-8}T+0.89\ T^{-2}$, and their values at ambient conditions is $8.30\times10^{-6}\,K^{-1}$ and $5.96\times10^{-6}\,K^{-1}$, respectively.

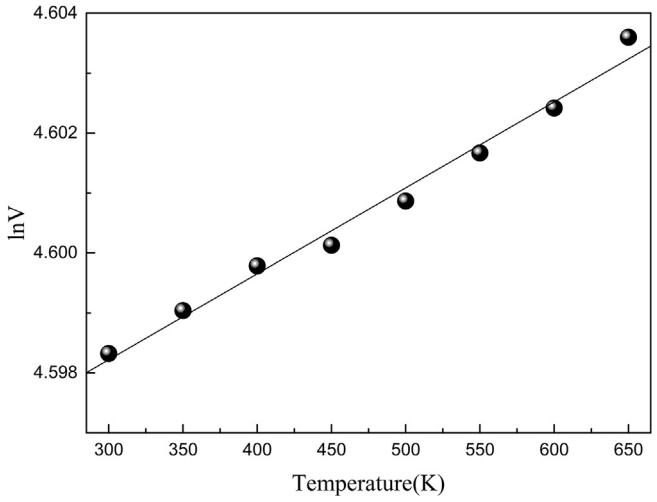

Fig. 5. Thermal expansion coefficient of cadmium sulfide in wurtzite structure.

3.3. Pressure-volume-temperature data for RS phase of CdS

The third-order Birch-Murnaghan EoS was applied to our high-pressure and high-temperature data with the form as follows:

$$P=\frac{3}{2}K_T\left[(V_T/V)^{\frac{7}{3}}-(V_T/V)^{\frac{5}{3}}\right]\times\left[1+\frac{3}{4}\left(K'_T-4\right)\left[(V_T/V)^{\frac{2}{3}}-1\right]\right] \quad (3)$$

In this equation, the thermal dependences of the zero-pressure volume V_T and bulk modulus K_T at different isotherms are expressed using the following equations:

$$K_T=K_0+(\partial K/\partial T)_p(T-300) \quad (4)$$

where $(\partial K/\partial T)_p$ is the temperature derivative of the bulk modulus.

$$V_T=V_0 exp\int_{300}^{T}\alpha_T dT \quad (5)$$

where α_T is the coefficient of thermal expansion.

Generally, the thermal expansion should be assumed to be a linear function of temperature ($\alpha_T=\alpha_0+\alpha_1 T$). However, because of the limited *P-T* data points in this study and the relatively narrow range of temperature (300–650 K), it is difficult to acquire the α_1. Here, we assumed α_T as a constant over the temperature range. By using the console program of *EosFit 5.2* [31], we obtained the thermal expansion coefficient of RS cadmium sulfides $\alpha_0=2.97\ (25)\times10^{-5}\,K^{-1}$.

4. Discussions

4.1. Phase transition boundary of CdS

Due to the CdS is an important optoelectronic material, numerous studies have been focused on the phase transition of CdS at high pressure [10–26]. It was found that the pressure-induced phase transition of CdS from WZ phase to RS phase occurred at about 2.0–3.5 GPa. The phase transition pressure obtained from this study is 2.6 GPa, which is consistent with the previous results. And by unloading the pressure from high pressures to ambient conditions in this study, the sample recovered as WZ phase, which indicated that the WZ-RS phase transition of CdS is reversible. Furthermore, in this study, the WZ-RS phase transition of CdS finished completely at 2.6 GPa and WZ-RS phase coexistence was not founded (Fig. 2B), which is similar to the results of Sowa [19]. He reported that WZ-type CdS powder transformed to the RS phase at 2.54 GPa, and the region of two coexisting phases was narrow and at 2.70 GPa only a very small amount of the WZ phase was observed. However, our results are slightly different from the results of Li et al. [22] who argued the WZ-RS phase transition of CdS occurred at 3.0 GPa and was completed at 4.3 GPa. As a comparison, the pressure-transmitting medium of *P-V* experiments used in this study is neon gas that is different from what Li et al. [22] used (a 16:4:1 mixture methanol-ethanol-water). This may be the main reason to make the phase transition pressure in this study slightly different from that of Li et al. In addition, whether it has a mixed WZ-RS structure in the WZ-RS phase transition process was not definitely determined in this study, because in the present case the initial pressure in the sample chamber was 2.6 GPa after Ne was filled in the sample chamber [37], at which the phase transition may have been completely finished and the mixed WZ-RS structure may not be observed. But according to the previous literature [10,11,22], the mixed WZ-RS structure was still existed when the pressure exceeds 2.6 GPa, so we tend to believe that there is no mixed phase in the WZ-RS phase transition process.

The phase transitions of cadmium chalcogenides have been investigated extensively and the phase transition pressures of CdSe and CdTe have also been determined at high pressure. For example, the phase transition pressure of CdSe transforming from WZ type to RS type is ~2.7 GPa [10,38], and CdTe transforming from ZB type to RS type is about 3.9 GPa [10,39]. Comparing the phase transition pressures of CdS, CdSe and CdTe from WZ (or ZB) type to RS type, one can conclude that the phase transition pressures of CdS and CdSe are very close, while the phase transition pressures of CdTe is only slightly larger than that of CdS and CdSe. It was because that CdS and CdSe have the WZ structure, while CdTe has the ZB structure at ambient conditions. This phenomenon is quite different not only from lead chalcogenides (PbS, PbSe and PbTe), but also from mercury chalcogenides (HgS, HgSe and HgTe) and zinc chalcogenides (ZnS, ZnSe and ZnTe). In these chalcogenides, their phase transition pressures reduce significantly in turn with the increasing atomic number in anion [40]. For instance, the phase transition pressure of lead chalcogenides transformed from RS type to CsCl type are 25.0 GPa, 20.0 GPa and 14.0 GPa, respectively [41]; the mercury chalcogenides transformed from the ZB type to RS type at 20 GPa [42], 15 GPa [43] and 8 GPa [44], respectively; and the zinc chalcogenides transformed from the ZB type to RS type at 15 GPa [45], 13.5 GPa [46] and 11.9 GPa [47], respectively.

4.2. Thermoelastic properties of CdS and compared with CdSe and CdTe

The elastic properties of CdS have been studied frequently in the last few decades (Table 3). As can be seen from Table 3, the bulk modulus values (K_0) of CdS are not always consistent but between 78.4 and 105 GPa [18,20–22,24,48]. Compared with the earlier experimental results, the K_0 of CdS in the RS phase obtained from this study agrees approximately with result determined by Suzuki et al. [24], but slightly smaller than the result obtained by Li et al. [22]. Moreover, the K_0 of CdS determined by the theoretical calculation earlier are 92.5–97.28 GPa (Table 3), which are all larger than that of this study. Relative to the accuracy of the data in the previous studies, the accuracy of the data points collected in this study is unprecedented. And the III-BM EoS fitting results for RS phase of CdS in this study have been verified by the F_E-f_E diagram (Fig. 4), indicating that the results in this study may be more reliable. As may be expected, the RS phase of CdS is distinctly more uncompressible than the WZ phase with $K_0 = 62.8$ (8) GPa and $K'_0 = 4$ (fixed) [19]. In addition, comparing the bulk moduli for RS type of CdS, CdSe and CdTe, we observed that the bulk moduli reduce in turn with the increasing atomic number in anion (Table 3). We infer that there are two possible sources for this situation. First, the ionic radii of S^{2-}, Se^{2-} and Te^{2-} increase [S^{2-} (1.84 Å) < Se^{2-} (1.91 Å) < Te^{2-} (2.11 Å)]. Second, the electronegativity of S, Se and Te decrease [S (2.58) > Se (2.55) > Te (2.1)]. The details of the discussion were described in the following.

To the best knowledge of the authors, there are not any reports about the thermal expansion of CdS. In this study, we obtained the thermal expansion $\alpha_T = -4.13 \times 10^{-5} + 8.86 \times 10^{-8} T + 2.68\ T^{-2}$ for WZ phase of CdS, and the α_T of WZ phase of CdS at ambient conditions is $1.51 \times 10^{-5}\ K^{-1}$. Furthermore, we also obtained the axial thermal expansivities of CdS in WZ phase along *a*-axis and *c*-axis is $\alpha_{aT} = -3.71 \times 10^{-5} + 6.43 \times 10^{-8} T + 2.35\ T^{-2}$ and $\alpha_{cT} = -1.05 \times 10^{-5} + 2.19 \times 10^{-8}\ T + 0.89\ T^{-2}$, and their values at ambient conditions is $8.30 \times 10^{-6}\ K^{-1}$ and $5.96 \times 10^{-6}\ K^{-1}$, respectively. It can be inferred that the *a*-axis of WZ-type CdS is more expansible than the *c*-axis with the increasing temperature. In addition, the thermal expansivity of RS phase of CdS obtained here is $\alpha_0 = 2.97\ (25) \times 10^{-5}\ K^{-1}$.

4.3. Influence factors on bulk modulus of metal sulfide (CdS, ZnS, HgS and PbS)

ZnS, CdS, HgS and PbS have the same rocksalt phase at high pressure, which gives us a good opportunity to investigate the influence of cations on the bulk modulus of metal sulfide in rocksalt phase. The elastic properties of ZnS, CdS, HgS and PbS in the RS phase were compared in Table 3.

In the RS phase, the K_0 of ZnS is between 83.1 and 117.6 GPa [49–57], and most of them are theoretical calculation results (Table 3), only Ves et al. [56], Zhou et al. [57] and Desgreniers et al. [50] obtained the K_0 of ZnS by XRD experiments. Ves et al. [56] used a DAC to investigate the phase transition of natural single crystals ZnS by XRD method at pressure up to 27 GPa, and the bulk modulus of ZnS in RS phase estimated by Ves et al. is 103.6 (60) GPa, with fixed K'_0 at 4. Their result is more agreement with the theoretical calculation results (Table 3). Subsequently, Zhou et al. [57] measured the static compressibility of the RS phase of polycrystalline ZnS at room temperature using XRD through a DAC between 11 and 45 GPa, and obtained the $K_0 = 85.0$ (38) GPa with $K'_0 = 4$ (fixed). The K_0 obtained by Zhou et al. is slightly smaller than the results of theoretical calculated. Then, Desgreniers et al. [50] studied the structural parameters and EoS of synthetic ZnS by XRD using synchrotron radiation for pressures below 96 GPa, and obtained the $K_0 = 117.6$ GPa, with $K'_0 = 4$ (fixed). Their results are obviously larger than that of other investigators (Table 3).

According to the previous literature, the K_0 of PbS in RS phase is between 51.0 and 66.4 GPa [41,58–61], and most of them are also theoretical calculation results except the result of Knorr et al. [58],

Table 3
Elastic parameters of metal sulfide (XS, X = Zn,Hg,Pb,Cd)in rocksalt phase

Sample	V_0(Å^3)	K_0(GPa)	K'_0	Method	Reference
ZnS	135.01	85.0 (38)	4(fixed)	XRD	Zhou et al.(1991) [57]
	129.55	103.6(60)	4(fixed)	XRD	Ves et al.(1990) [56]
	_	117.6	4(fixed)	XRD	Desgreniers et al.(2000) [50]
	_	96.2	4.35	XRD	Desgreniers et al.(2000) [50]
	132.18	100.1	4.05	LMTO-LDA	Ves et al.(1990) [56]
	_	105(6)	3.8(1)	Inclined-mirror	Uchino et al.(1999) [55]
	126.51	104.4	4.29	PP-LDA	Nazzal and Qteish(1996) [53]
	121.29	107.6	4.1	NLCC	Nazzal and Qteish(1996) [53]
	141.42	83.1	10	HF-LCAO	Jaffe et al.(1993) [52]
	130.32	89.54	4.58	GGA	Chen et al.(2006) [49]
	131.56	95.89	–	TB-LMTO	Gangadharan et al.(2003) [51]
	126.28	104.4	4.28	PP-PW	Qteish and Parrinello(2000) [54]
CdS	153.82	92.5	4.8	LDA/USP	Tan et al.(2011) [21]
	153.36	97.28	4.5101	FP/LMTO	Benkhettou et al.(2004) [20]
	161.88	94.74	3.802	ab initio	Knudson et al.(1999) [18]
	156.59	95	3.99	DFT-LDA	Chen et al.(2011) [48]
	161.1	86.7	4.36	XRD	Suzuki et al.(1983) [24]
	157.3	105(2)	4(fixed)	XRD	Li et al. (2013) [22]
	162.25(7)	78.4(4)	4(fixed)	XRD	This study
	162.0(1)	81.6(13)	3.68(13)	XRD	This study
CdSe	186.62(7)	63.6(4)	4.64(4)	GGA	Li et al.(2014) [37]
	173.28(1)	78.98(7)	4.752(6)	LDA	Li et al.(2014) [37]
CdTe	207.47	63.82	5.01	LDA	Kabita et al. [39]
	228.10	48.24	4.99	GGA	Kabita et al. [39]
HgS	128.927	67.25	4.56	FP	Sun and Dong(2005) [62]
PbS	216.65	56.0	3.6	FP-LMTO	Ahuja(2003) [41]
	_	51.0(1.2)	4.3(9)	XRD	Knorr et al.(2003) [58]
	_	52.43(9)	4.69(2)	DFT	Knorr et al.(2003) [58]
	217.30	53.3	4.637	GGA	Lach-hab et al.(2002) [59]
	201.23	64.8	4.291	LDA	Lach-hab et al.(2002) [59]
	206.01	66.3	4.38	LAPW	Wei and Zunger.(1997) [61]
	_	66.4	4.38691	LDA	Rached et al.(2003) [60]

FP: the first-principles computation; LMTO-LDA: LMTO-LDA total-energy calculation; NLCC: nonlinear exchange-correlation core corrections; HF-LCAO: hartree-fock and linear-combination-of-atomic-orbitals method; TB-LMTO: the tight binding linear muffin tin orbital method; GGA: generalized gradient approximation; PP-PW: a first-principles pseudopotential plane-wave method; FP-LMTO: the full potential linear-muffin-tin-orbital method; DFT: density functional theory; LAPW: the linearized augmented plane wave method; LAD: local density approximation; USP: Vanderbilt-type ultra-soft pseudopotentials; LMTO: Linear Muffin-Tin Orbital; FP/LMTO: full-potential linear muffin-tin-orbital.

who have investigated the high-pressure behavior of PbS by angular dispersive X-ray powder diffraction up to pressures of 6.8 GPa, and obtained the $K_0 = 51.0$ (1.2) GPa, with $K'_0 = 4.3$ (9) which are consistent with the theoretical results. However, as for the RS phase of HgS, only Sun and Dong [62] calculated the K_0 of HgS in the RS phase which is 67.25 GPa, based on the first principle. In general, with the increase of cationic atomic number, the K_0 of ZnS, CdS, HgS and PbS decrease in turn. The reason may be complicated.

Initially, the ionization energy of the conduction electrons for the cation may affect the K_0 of these compounds. It is believed that the effective potential for the valence electrons and the conducting electrons of larger atoms become weaker because the larger atom numbers means that a larger number of core electrons [63]. This leads to the fact that the ionization energy of the conduction electrons for the heavier atom in the same group of the periodic table of the elements is smaller [63]. Thus, with the increase of cationic atomic number, the compounds are easily compressed [40].

Then, the cationic radius may also have an effect on the bulk modulus of different metal sulfides. The ion radii of Zn^{2+} (0.074 nm), Cd^{2+} (0.095 nm), Hg^{2+} (0.102 nm) and Pb^{2+} (0.119 nm) increase in order of increasing atomic number and the relationship between ion radius and bulk modulus is shown in Fig. 6. In order to compare the bulk modulus of these sulfides, the bulk moduli determined by previous XRD experiments are chosen as much as possible in the diagram. Therefore, the bulk modulus of CdS is $K_0 = 78.4$ (4) GPa with $K'_0 = 4$ from this experiment. Because the K_0 of ZnS obtained by Ves et al. [56] is more consistent with the theoretical results than the results of Zhou et al. and Desgreniers et al. (Table 3), the XRD results of Ves et al. [56] for ZnS ($K_0 = 103.6$ (60) GPa with $K'_0 = 4$) is chosen to discuss in the following. As the bulk modulus of HgS ($K_0 = 67.25$ GPa with $K'_0 = 4.56$) we know from earlier literature is only the results of Sun and Dong [62] calculated by using the first principle, we have no choice but to

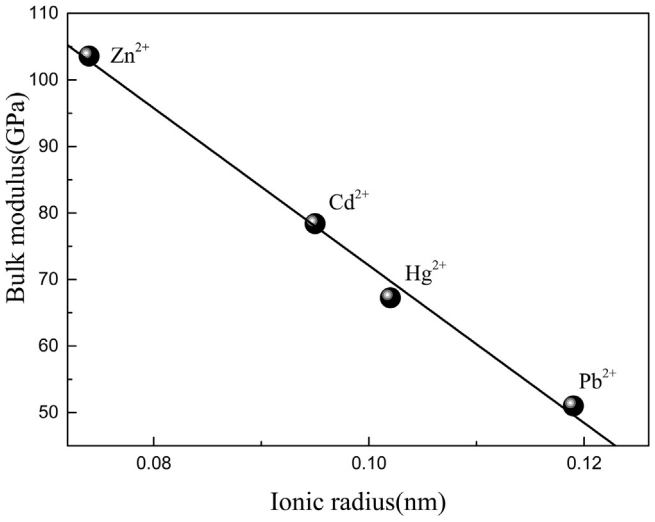

Fig. 6. Variations of the bulk modulus of metal sulfides against ionic radius in rocksalt structure.

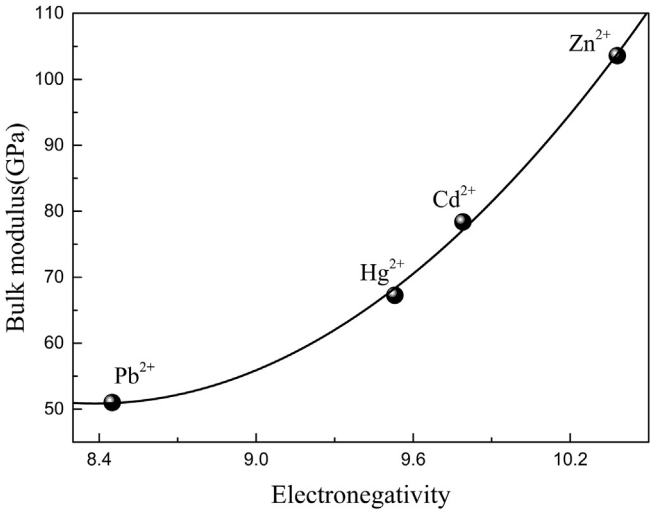

Fig. 7. Variations of the bulk modulus of metal sulfides against electronegativity in rocksalt structure.

choose it to discuss in the following. And the data of PbS ($K_0 = 51.0(1.2)$ GPa with $K'_0 = 4.3\ (9)$) is from the only XRD results of Knorr et al. [58]. From the Fig. 6, it was known that the bulk modulus of the metal sulfide in the rocksalt phase decreases gradually with the cationic radius increases. Moreover, the data show a good linear correlation and the fitting equation is $K_0 = 190.4\ (64) - 1183.0\ (649)\ r$, and the R-squared is 0.99103, where K_0, r represent the zero-pressure isothermal bulk modulus and the cationic radius.

At last, the electronegativity of element may also be an important reason for the change in bulk modulus [64]. Electronegativity is a chemical property that describes the ability of an atom to attract electrons. An atom's electronegativity is affected by its atomic weight and the distance of its valence electrons from the charged nucleus [65]. With the increase of the element electronegativity, the attraction of the atoms during the formation of the chemical bond is heightened, thus the electron density between the cation and the anion is also heightened, resulting in more compressible for the crystal [65]. The electronegativity of Zn^{2+}, Cd^{2+}, Hg^{2+} and Pb^{2+} is 10.38, 9.79, 9.53 and 8.45, respectively. Fig. 7 shows the relationship between the electronegativity and the bulk modulus. As we can know from Fig. 7, with the decrease of electronegativity, the bulk modulus of the metal sulfide in the rocksalt structure becomes smaller. By fitting the experimental data with a binomial, we obtained the equation of $K_0 = 986.5\ (172) - 223.2\ (369)\ \chi + 13.3(20)\ \chi^2$, and the R-squared is 0.9943, where K_0, χ represent the zero-pressure isothermal bulk modulus and the electronegativity of element.

In summary, with the ionization energy of the conduction electrons and electronegativity increases, or the cationic radius decrease, the bulk modulus of metal sulfide gradually increases. Furthermore, it has a good linear relationship between bulk modulus and cationic radius. Since the cationic radius and electronegativity mainly affect the bond strength of the ionic bond, the smaller the cationic radius is, the greater the electronegativity and bond strength of the ionic bond are. Therefore, in the rocksalt structure of the metal sulfide, the value of the bulk modulus and the electronegativity of the cation have a positive correlation.

5. Conclusions

The phase transition and elastic properties of CdS were studied at high temperature and high pressure (up to 650 K and 21.9 GPa) by using *in situ* synchrotron radiation X-ray diffraction experiments. As pressure increases to about 2.6 GPa, CdS undergoes a phase transition from WZ to RS phase completely, and a mixed phase has not been observed in this process, the CdS still existed stably in RS phase at the maximum pressure up to 21.9 GPa in this study. Moreover, this study also indicated the WZ-RS phase transition of CdS was reversible. In addition, we calculated the *P-V* data of RS phase of CdS at room temperature and high pressure, using the III-BM EoS, and obtained the bulk modulus $K_0 = 81.6\ (13)$ GPa and its pressure derivative $K'_0 = 3.68\ (13)$. Simultaneously, we also obtained the thermal expansion of the WZ phase ($1.51 \times 10^{-5} K^{-1}$) and RS phase ($2.97\ (25) \times 10^{-5}\ K^{-1}$) of CdS for the first time. Based on the comparison of the phase transition pressure from WZ type to RS type of cadmium chalcogenides (CdS, CdSe and CdTe), it was found that the phase transition pressure is quite similar for them. We also discussed the effect of different metal cations on the bulk modulus of metal sulfide in the RS phase, where the bulk modulus is negatively correlated with the ion radius of metal cation and positively correlated with the electronegativity.

Acknowledgements

This work is supported by the National Natural Science Foundation of China (Grant No. 41772043 and 41374107), the Joint Research Fund in Huge Scientific Equipment (U1632112) under cooperative agreement between NSFC and CAS, CAS "Light of West China" Program (Dawei Fan, 2017), Youth Innovation Promotion Association CAS (Dawei Fan, 2018), and the CPSF-CAS Joint Foundation for Excellent Postdoctoral Fellows (Grant No. 2017LH014). The high-pressure X-ray diffraction experiments were performed at the High-Pressure Experiment Station (4W2), Beijing Synchrotron Radiation Facility (BSRF), and the BL15U1 of the Shanghai Synchrotron Radiation Facility (SSRF).

References

[1] M.O. Schwartz, Cadmium in zinc deposits: economic geology of a polluting element, Int. Geol. Rev. 42 (2000) 445–469.
[2] P. Zhou, Z.F. Liu, X.Q. Wang, M. Zhou, C.H. Hu, Z. Zheng, J.H. Wu, First-principle study of phase stability, electronic structure and thermodynamic properties of cadmium sulfide under high pressure, J. Phys. Chem. Solid. 75 (2014) 662–669.
[3] U. Hotje, C. Rose, M. Binnewies, Lattice constants and molar volume in the system ZnS, ZnSe, CdS, CdSe, Solid State Sci. 5 (2003) 1259–1262.
[4] D. Lincot, G. Hodes, Chemical solution deposition of semiconducting and non-metallic films, in: Proceedings of the International Symposium, in, the Electrochemical Society, 2006.
[5] D. Reynolds, G. Leies, L. Antes, R. Marburger, Photovoltaic effect in cadmium sulfide, Phys. Rev. 96 (1954) 533.
[6] A. Luque, S. Hegedus, Handbook of Photovoltaic Science and Engineering, Wiley, 2003.
[7] R. Agarwal, C.J. Barrelet, C.M. Lieber, Lasing in single cadmium sulfide nanowire optical cavities, Nano Lett. 5 (2005) 917–920.
[8] W.J. Minkus, Temperature dependence of the pyroelectric effect in cadmium sulfide, Phys. Rev. 138 (1965) A1277–A1287.
[9] H.M. Smith, High Performance Pigments, 2002.
[10] A. Edwards, H. Drickamer, Effect of pressure on the absorption edges of some III-V, II-VI, and I-VII compounds, Phys. Rev. 122 (1961) 1149.
[11] G.A. Samara, H.G. Drickamer, Pressure induced phase transitions in some II–VI compounds, J. Phys. Chem. Solid. 23 (1962) 457–461.
[12] N.B. Owen, P.L. Smith, J.E. Martin, A.J. Wright, X-ray diffraction at ultra-high pressures, J. Phys. Chem. Solid. 24 (1963) 1519–1520.
[13] G. Samara, A. Giardini, Compressibility and electrical conductivity of cadmium sulfide at high pressures, Phys. Rev. 140 (1965) A388.
[14] C.F. Cline, D.R. Stephens, Volume compressibility of BeO and other II-VI compounds, J. Appl. Phys. 36 (1965) 2869–2873.
[15] U. Venkateswaran, M. Chandrasekhar, H. Chandrasekhar, Luminescence and Raman spectra of CdS under hydrostatic pressure, Phys. Rev. B 30 (1984) 3316.
[16] U. Venkateswaran, M. Chandrasekhar, Low-temperature studies of the photoluminescence in CdS under hydrostatic pressure, Phys. Rev. B 31 (1985) 1219–1222.
[17] B. Batlogg, A. Jayaraman, J.E. Van Cleve, R.G. Maines, Optical absorption, resistivity, and phase transformation in CdS at high pressure, Phys. Rev. B 27 (1983) 3920–3923.

[18] M. Knudson, Y. Gupta, A. Kunz, Transformation mechanism for the pressure-induced phase transition in shocked CdS, Phys. Rev. B 59 (1999) 11704.
[19] H. Sowa, On the mechanism of the pressure-induced wurtzite- to NaCl-type phase transition in CdS: an X-ray diffraction study, Solid State Sci. 7 (2005) 73–78.
[20] N. Benkhettou, D. Rached, B. Soudini, M. Driz, High-pressure stability and structural properties of CdS and CdSe, Phys. Stat. Sol. B Basic Res. 241 (2004) 101–107.
[21] J. Tan, Y. Li, G. Ji, High-pressure phase transitions and thermodynamic behaviors of cadmium sulfide, Acta Phys. Pol., A 120 (2011) 501–506.
[22] Y.C. Li, X.N. Zhang, H. Li, X.D. Li, C.L. Lin, W.S. Xiao, J. Liu, High pressure-induced phase transitions in CdS up to 1 Mbar, J. Appl. Phys. 113 (2013) 5.
[23] J. Oscgi, K. Shimizu, T. Nakamura, A. Onodera, High pressure transition in cadmium sulfide, Rev. Phys. Chem. Jpn. 36 (1966).
[24] T. Suzuki, T. Yagi, S.i. Akimoto, T. Kawamura, S. Toyoda, S. Endo, Compression behavior of CdS and BP up to 68 GPa, J. Appl. Phys. 54 (1983) 748–751.
[25] X.-S. Zhao, J. Schroeder, T.G. Bilodeau, L.-G. Hwa, Spectroscopic investigations of CdS at high pressure, Phys. Rev. B 40 (1989) 1257–1264.
[26] Y. Wang, J. Zhang, C. Wang, C. Li, C. Gao, Semicomductor-metal-semiconductor phase transition of CdS under high pressure, Chalcogenide Lett. 12 (2015) 357–362.
[27] J. Xiao, B. Wen, R. Melnik, Y. Kawazoe, X. Zhang, Phase transformation of cadmium sulfide under high temperature and high pressure conditions, Phys. Chem. Chem. Phys. 16 (2014) 14899–14904.
[28] R.J. Hemley, C.S. Zha, A.P. Jephcoat, H.K. Mao, L.W. Finger, D.E. Cox, X-ray-diffraction and equation of state of sold neon to 110 GPa, Phys. Rev. B 39 (1989) 11820–11827.
[29] T. Holland, S. Redfern, Unit cell refinement from powder diffraction data: the use of regression diagnostics, Mineral. Mag. 61 (1997) 65–77.
[30] A. Hammersley, S. Svensson, M. Hanfland, A. Fitch, D. Hausermann, Two-dimensional detector software: from real detector to idealised image or two-theta scan, Int. J. High Pressure Res. 14 (1996) 235–248.
[31] R.J. Angel, Equations of state, Rev. Mineral. Geochem. 41 (2000) 35–59.
[32] D. Fan, W. Zhou, S. Wei, Y. Liu, M. Ma, H. Xie, A simple external resistance heating diamond anvil cell and its application for synchrotron radiation X-ray diffraction, Rev. Sci. Instrum. 81 (2010), 053903.
[33] Y. Fei, A. Ricolleau, M. Frank, K. Mibe, G. Shen, V. Prakapenka, Toward an internally consistent pressure scale, Proc. Natl. Acad. Sci. Unit. States Am. 104 (2007) 9182–9186.
[34] R.J. Angel, M. Bujak, J. Zhao, G.D. Gatta, S.D. Jacobsen, Effective hydrostatic limits of pressure media for high-pressure crystallographic studies, J. Appl. Crystallogr. 40 (2007) 26–32.
[35] F. Birch, Finite elastic strain of cubic crystals, Phys. Rev. 71 (1947) 809.
[36] Y. Fei, Thermal expansion, Mineral Physics & Crystallography: a Handbook of Physical Constants, 1995, pp. 29–44.
[37] Y. Li, C. Lin, G. Li, J. Xu, X. Li, J. Liu, Structure determination of the high-pressure phase of CdSe, J. Appl. Phys. 115 (2014), 223507.
[38] H. Sowa, The high-pressure behaviour of CdSe up to 3 GPa and the orientation relations between its wurtzite- and NaCl-type modifications, Solid State Sci. 7 (2005) 1384–1389.
[39] K. Kabita, J. Maibam, B.I. Sharma, R.K.B. Singh, R.K. Thapa, First principles phase transition, elastic properties and electronic structure calculations for cadmium telluride under induced pressure: density functional theory, LDA, GGA and modified Becke-Johnson potential, Mater. Res. Express 3 (2016) 11.
[40] F. Da-Wei, Z. Wen-Ge, W. Shu-Yi, L. Jing, L. Yan-Chun, J. Sheng, X. Hong-Sen, Phase relations and pressure-volume-temperature equation of state of galena, Chin. Phys. Lett. 27 (2010), 086401.
[41] R. Ahuja, High pressure structural phase transitions in IV–VI semiconductors, Phys. Status Solidi 235 (2003) 341–347.
[42] R. Nelmes, M. McMahon, Structural transitions in the group IV, III-V, and II-VI semiconductors under pressure, Semiconduct. Semimet. 54 (1998) 145–246.
[43] T. Huang, A. Ruoff, Pressure-induced phase transition of HgS, J. Appl. Phys. 54 (1983) 5459–5461.
[44] A. Ohtani, T. Seike, M. Motobayashi, A. Onodera, The electrical properties of HgTe and HgSe under very high pressure, J. Phys. Chem. Solid. 43 (1982) 627–632.
[45] S. Yu, I. Spain, E. Skelton, High pressure phase transitions in tetrahedrally coordinated semiconducting compounds, Solid State Commun. 25 (1978) 49–52.
[46] G. Itkin, G.R. Hearne, E. Sterer, M.P. Pasternak, W. Potzel, Pressure-induced metallization of ZnSe, Phys. Rev. B 51 (1995) 3195.
[47] K. Strössner, S. Ves, C.K. Kim, M. Cardona, Pressure dependence of the lowest direct absorption edge of ZnTe, Solid State Commun. 61 (1987) 275–278.
[48] H. Chen, Y. Zhu, B. Wu, High pressure polymorph of CdS predicted by first principles, Phys. B Condens. Matter 406 (2011) 4052–4055.
[49] X.-R. Chen, X.-F. Li, L.-C. Cai, J. Zhu, Pressure induced phase transition in ZnS, Solid State Commun. 139 (2006) 246–249.
[50] S. Desgreniers, L. Beaulieu, I. Lepage, Pressure-induced structural changes in ZnS, Phys. Rev. B 61 (2000) 8726.
[51] R. Gangadharan, V. Jayalakshmi, J. Kalaiselvi, S. Mohan, R. Murugan, B. Palanivel, Electronic and structural properties of zinc chalcogenides ZnX (X= S, Se, Te), J. Alloy. Comp. 359 (2003) 22–26.
[52] J. Jaffe, R. Pandey, M. Seel, Ab initio high-pressure structural and electronic properties of ZnS, Phys. Rev. B 47 (1993) 6299.
[53] A. Nazzal, A. Qteish, Ab initio pseudopotential study of the structural phase transformations of ZnS under high pressure, Phys. Rev. B 53 (1996) 8262.
[54] A. Qteish, M. Parrinello, Stability and structural properties of the SC16 phase of ZnS under high pressure, Phys. Rev. B 61 (2000) 6521.
[55] M. Uchino, T. Mashimo, M. Kodama, T. Kobayashi, E. Takasawa, T. Sekine, Y. Noguchi, H. Hikosaka, K. Fukuoka, Y. Syono, T. Kondo, T. Yagi, Phase transition and EOS of zinc sulfide (ZnS) under shock and static compressions up to 135 GPa, J. Phys. Chem. Solid. 60 (1999) 827–837.
[56] S. Ves, U. Schwarz, N. Christensen, K. Syassen, M. Cardona, Cubic ZnS under pressure: optical-absorption edge, phase transition, and calculated equation of state, Phys. Rev. B 42 (1990) 9113.
[57] Y.H. Zhou, A.J. Campbell, D.L. Heinz, Equations of state and optical-properties of the high-pressure phase of zinc-sulfide, J. Phys. Chem. Solid. 52 (1991) 821–825.
[58] K. Knorr, L. Ehm, M. Hytha, B. Winkler, W. Depmeier, The high-pressure α/β phase transition in lead sulphide (PbS), The Europ. Phys. J. B-Condens. Matter Complex Syst. 31 (2003) 297–303.
[59] M. Lach-hab, D.A. Papaconstantopoulos, M.J. Mehl, Electronic structure calculations of lead chalcogenides PbS, PbSe, PbTe, J. Phys. Chem. Solid. 63 (2002) 833–841.
[60] D. Rached, M. Rabah, N. Benkhettou, M. Driz, B. Soudini, Calculated band structures and optical properties of lead chalcogenides PbX (X= S, Se, Te) under hydrostatic pressure, Phys. B Condens. Matter 337 (2003) 394–403.
[61] S.-H. Wei, A. Zunger, Electronic and structural anomalies in lead chalcogenides, Phys. Rev. B 55 (1997) 13605.
[62] S.-R. Sun, Y.-H. Dong, First-principles study of the phase transition of HgS from cinnabar to rocksalt structure under high pressure, Phys. Rev. B 72 (2005), 174101.
[63] A. Hao, C. Gao, M. Li, C. He, X. Huang, D. Zhang, C. Yu, H. Liu, Y. Ma, Y. Tian, A study of the electrical properties of HgS under high pressure, J. Phys. Condens. Matter 19 (2007), 425222.
[64] J. Zhang, Room-temperature compressibilities of MnO and CdO: further examination of the role of cation type in bulk modulus systematics, Phys. Chem. Miner. 26 (1999) 644–648.
[65] L.C. Allen, Electronegativity is the average one-electron energy of the valence-shell electrons in ground-state free atoms, J. Am. Chem. Soc. 111 (1989) 9003–9014.